Viscosity-modulated breakup and coalescence of large drops in bounded turbulence

Alessio Roccon,[1,2] Marco De Paoli,[1] Francesco Zonta,[1] and Alfredo Soldati[1,2,*]
[1]*Institute of Fluid Mechanics and Heat Transfer, TU-Wien, 1060 Vienna, Austria*
[2]*Polytechnic Department, University of Udine, 33100 Udine, Italy*
(Received 8 February 2017; published 25 August 2017)

In this work, we examine the influence of viscosity on breakup and coalescence of a swarm of large drops in a wall-bounded turbulent flow. We consider several values of surface tension and a wide range of drops to fluid viscosity ratios $\lambda = \eta_d/\eta_c$ (with η_d the viscosity of the drops and η_c the viscosity of the carrier fluid), from $\lambda = 0.01$ to $\lambda = 100$, while we maintain the same density for drops and carrier fluids. Drops can coalesce and break following a complex dynamics that is primarily controlled by the interplay between turbulence fluctuations (measured by Reynolds number, Re_τ), surface tension (measured by Weber number, We), and λ. We use direct numerical simulation of turbulence coupled with a phase field method to describe the drops dynamics. We consider three different values of We (which is the inverse of the surface tension): We = 0.75, 1.5, and 3. For each value of We, we assume five values of λ: $\lambda = 0.01$, 0.1, 1, 10, and 100. We observe a consistent action of increasing λ, which, especially for the larger Weber numbers, decreases significantly the breakup rate of the drops. Qualitatively, an increase of drop viscosity decreases the breakup rate, very much like an increase of surface tension does. The mechanism by which drop viscosity acts is a modulation of turbulence fluctuations inside the drop, which reduces the work surface tension has to do to preserve drop integrity. We believe that this may give important indications in many industrial applications to control drop coalescence and fragmentation via the ratio of drop to fluid viscosity.

DOI: 10.1103/PhysRevFluids.2.083603

I. INTRODUCTION

Prediction of breakup and coalescence rates of a swarm of liquid drops immersed in a turbulent liquid flow (liquid-liquid emulsion) is crucially dependent on a number of hard-to-tackle factors. Among many others these include turbulence, turbulence-interface interactions, surface tension effects, and viscosity gradients. Each of these effects has a specific action on breakup and coalescence, and we can envision drop dynamics as the ultimate result of a complex competition between destabilizing and stabilizing effects. Destabilizing effects are primarily due to the combined effects of fluctuating inertial and shear terms acting at the drop interface. Stabilizing effects are due to surface tension, which is a restoring force acting to preserve drop sphericity. The outcome of this competition determines drop deformation, breakage, and coalescence. In this picture, viscosity gradients across the interface of the drops can act as modulators of the localized shear stresses and can amplify or damp the initial turbulence perturbations to the point of changing profoundly the final result.

Drop coalescence and breakup is of paramount importance in many environmental and industrial applications, from transport of pollutant drops in water bodies [1] to hydrocarbon separation or oil-water emulsions in chemical plants and the petroleum industry [2–4]. In this paper we focus precisely on liquid-liquid emulsions, in which drops of one phase are dispersed within the other phase.

In this instance, the knowledge of the drop number density and/or the drop interface extension is a key parameter to optimize the design of efficient oil separators, in which drop coalescence should be promoted and drop fragmentation reduced.

*Author to whom correspondence should be addressed: alfredo.soldati@tuwien.ac.at

For drop breakup in turbulence, the literature dates back to the seminal work of Hinze [5], who modeled the mechanism of liquid drops splitting in a turbulent gas environment. Since the fundamental physics of drops splitting in gas-liquid or liquid-liquid configurations is controlled by the same parameters, results obtained for the gas-liquid case have been historically (and successfully) applied to the liquid-liquid case as well. In accordance with Hinze [5], drop breakup occurs when the Weber number We (i.e., the ratio between inertia and surface tension) exceeds a critical value, $\mathrm{We}_{\mathrm{cr}}$. Assuming a drop size in the inertial range of turbulence (so that Kolmogorov's law can be used to define turbulence fluctuations at the drop scale), Hinze [5] was able to predict the maximum size of a drop that will not be broken by turbulence in a given flow. Based on available experimental data [6,7], Hinze [5] finally proposed $\mathrm{We}_{\mathrm{cr}} = 1.18$, even though a general agreement on the value of $\mathrm{We}_{\mathrm{cr}}$ is still to be found (the value of $\mathrm{We}_{\mathrm{cr}}$ ranges between 1 and 12, largely depending on the employed fluids and on the flow configuration). Many subsequent theoretical and experimental studies (see [8–11], among others) have been performed on drop size distribution in engineering-relevant situations (liquid-liquid emulsions in pipelines and stirred tanks), with most of these studies conducted in dilute conditions, so to neglect drop coalescence. However, in any practical situation, drop breakup and coalescence occur simultaneously and cannot be neglected when a complete characterization of the drop swarm dynamics is required [12].

Unlike the case of drop breakup, drop coalescence has been the subject of relatively fewer studies, most of which focused on the binary collision of two separate drops in still fluid [13–15]. Although these studies have definitely provided useful insights to understand the fundamental physics of drop collisions and merging, their extension to more complex situations like drops moving inside turbulent pipes or reactors is not straightforward and still requires a leap forward [16,17].

From the previous literature survey it is apparent that a large proportion of the work on drop breakup and coalescence is based on experimental or theoretical approaches. This is due to the complex nature of drop interactions that has hindered the development of accurate numerical simulations of the phenomenon. Only recently, numerics has become available to analyze complex multiphase flow situations. Accurate numerical simulations can help provide the time evolution of the drop deformation together with the description of the entire flow field inside and outside of the drop. This is extremely important for unsteady turbulent flow conditions, where it is essential to record the coupled drop-turbulence interactions in time and space. In the literature we found only a few available direct numerical simulations [18–23] of the collective drop dynamics in turbulence. In this work we apply direct numerical simulation to the case of wall-bounded turbulence with fluids of different viscosities.

The aim of the present study is to extend available literature results on collective drop dynamics in wall-bounded turbulence considering the case of fluids with the same density but different viscosity. In particular, we consider a wide range of drop-to-fluid viscosity ratios $\lambda = \eta_d/\eta_c$ (with η_d the viscosity of the drops and η_c the viscosity of the carrier fluid), from $\lambda = 0.01$ to $\lambda = 100$.

This paper is organized as follows. We first describe the physical and numerical modeling used to perform the present simulations. Then, we present and discuss our numerical results, focusing in particular on the role of drop surface tension and drop viscosity on their coalescence and breakup efficiency. Finally, we use our numerical results to compute the value of the average drop diameter in turbulence, and we discuss our findings in view of the theory developed by Hinze [5].

II. METHODOLOGY

We consider a two-phase flow system composed by large drops with density ρ_d and dynamic viscosity η_d dispersed in a turbulent channel flow (with the carrier fluid being characterized by density ρ_c and dynamic viscosity η_c). The origin of the reference frame is located at the center of the channel and the x, y, and z axes point in the streamwise, spanwise, and wall-normal directions, respectively. The evolution of the two-phase flow system is described by a phase field method (PFM), which in recent years has been applied to this type of problem [20,24]. The method is based on the use of a single variable ϕ (order parameter) to describe the entire binary system: ϕ is uniform in the

bulk fluid regions ($\phi = \phi_+$ inside a drop and $\phi = \phi_-$ inside the carrier flow) and changes smoothly across the fluid-fluid interface. All the thermophysical properties of the fluids are proportional to the order parameter. The time evolution of the order parameter ϕ is described by the convective Cahn-Hilliard equation [25]:

$$\frac{\partial \phi}{\partial t} = -\mathbf{u} \cdot \nabla \phi + \mathcal{M} \nabla^2 \mu, \tag{1}$$

where $\mathbf{u}$ is the velocity field, $\mathcal{M}$ is the mobility parameter driving the interface relaxation, and μ is the chemical potential controlling the behavior of the interfacial layer and is defined in terms of a Ginzburg-Landau free energy functional:

$$\mathcal{F}[\phi, \nabla\phi] = \int_\Omega \left(f_0(\phi) + \frac{1}{2}\kappa |\nabla \phi|^2 \right) d\Omega. \tag{2}$$

The above expression of $\mathcal{F}[\phi, \nabla\phi]$, which is the sum of two different contributions, is used here to represent an immiscible binary mixture of isothermal fluids. In particular, $f_0(\phi)$ is the so-called double-well potential,

$$f_0(\phi) = \frac{\alpha}{4} \left(\phi_- + \sqrt{\frac{\beta}{\alpha}} \right)^2 \left(\phi_+ - \sqrt{\frac{\beta}{\alpha}} \right)^2, \tag{3}$$

which accounts for the tendency of the system to separate into the two pure stable phases. The second term, $\frac{1}{2}\kappa |\nabla \phi|^2$, in Eq. (2) is a nonlocal term (mixing energy) accounting for the energy stored in the interfacial layer. Note that α and β are two positive constants that define the interface properties, whereas κ is a positive parameter used to describe the magnitude of the surface tension. The time evolution of the order parameter ϕ is driven by the minimization of $\mathcal{F}[\phi, \nabla\phi]$ (i.e., by the chemical potential μ):

$$\mu = \frac{\delta \mathcal{F}[\phi, \nabla\phi]}{\delta \phi} = \alpha \phi^3 - \beta \phi - \kappa \nabla^2 \phi. \tag{4}$$

The Cahn-Hilliard equation [Eq. (1)] can be coupled with Navier-Stokes and continuity equations to form a model for the computation of a multiphase flow [26–28]. Using the half channel height h as a reference length, the shear velocity $u_\tau = \sqrt{\tau_w / \rho_c}$ (with τ_w the shear stress at the wall) as a reference velocity, and the bulk value $\phi_+ = \sqrt{\frac{\beta}{\alpha}}$ as a reference value of the order parameter, all the equations can be made dimensionless (with the superscript "+" indicating dimensionless variables being dropped for ease of reading), and the resulting set of equations is

$$\nabla \cdot \mathbf{u} = 0, \tag{5}$$

$$\frac{\partial \mathbf{u}}{\partial t} + \mathbf{u} \cdot \nabla \mathbf{u} = -\nabla p' + \nabla \Pi + \frac{1}{\mathrm{Re}_\tau} \nabla \cdot (r(\phi, \lambda)(\nabla \mathbf{u} + \nabla \mathbf{u}^{\mathbf{T}})) + \frac{3}{\sqrt{8}} \frac{\mathrm{Ch}}{\mathrm{We}} \nabla \cdot \tau_{\mathbf{c}}, \tag{6}$$

$$\frac{\partial \phi}{\partial t} + \mathbf{u} \cdot \nabla \phi = \frac{1}{\mathrm{Pe}} \nabla^2 \mu, \tag{7}$$

where the term $\frac{3}{\sqrt{8}} \frac{\mathrm{Ch}}{\mathrm{We}} \nabla \cdot \tau_{\mathbf{c}}$ represents the capillary force due to surface tension ($\tau_{\mathbf{c}} = |\nabla \phi|^2 \mathbf{I} - \nabla \phi \otimes \nabla \phi$ being the Korteweg stress), $\nabla \Pi$ is the mean pressure gradient driving the flow in the streamwise direction (kept constant during all the computations), and the function $r(\phi, \lambda)$ is a parameter that takes into account the viscosity variations between the two phases. Note that the Ginzburg-Landau free energy potential $\mathcal{F}[\phi, \nabla\phi]$ and the chemical potential μ in dimensionless form become

$$\mathcal{F}[\phi, \nabla\phi] = \tfrac{1}{4}(\phi - 1)^2 (\phi + 1)^2 + \tfrac{1}{2}\mathrm{Ch}^2 |\nabla \phi|^2, \tag{8}$$

$$\mu = \phi^3 - \phi - \mathrm{Ch}^2 \nabla^2 \phi. \tag{9}$$

The dimensionless groups in Eqs. (5)–(9) are defined as

$$\mathrm{Re}_\tau = \frac{\rho u_\tau h}{\eta_c}, \quad \mathrm{Pe} = \frac{u_\tau h}{\mathcal{M}}, \quad \mathrm{We} = \frac{\rho u_\tau^2 h}{\sigma}, \quad \mathrm{Ch} = \frac{\xi}{h}, \quad \lambda = \frac{\eta_d}{\eta_c}. \tag{10}$$

From a physical point of view, Re_τ (shear Reynolds number) is the ratio between inertial and viscous forces, whereas We is the ratio between inertial and surface tension forces. Note that increasing We increases the drop deformation (for $\mathrm{We} \to 0$ drops behave like rigid spheres). The Péclet number Pe is the ratio between diffusive and convective time scales of the interface, while the Cahn number Ch is the dimensionless thickness of the interface. The Cahn-Hilliard (6) and Navier-Stokes (7) equations are coupled through the capillary term, $\frac{3}{\sqrt{8}}\frac{\mathrm{Ch}}{\mathrm{We}}\nabla \cdot \tau_\mathbf{c}$, which models surface tension effects (momentum exchange occurring across the fluid-fluid interface) as volume forces acting on the very small volume region used to describe the interface (a thin transition region between the two bulk fluids).

The function $r(\phi,\lambda)$ in Eq. (6) is used to account for the nonuniform viscosity. In particular, assuming that the viscosity depends linearly on the order parameter ϕ [29,30], we have

$$r(\phi,\lambda) = \frac{(\lambda-1)(\phi+1)}{2}. \tag{11}$$

The governing equations are solved by a Fourier-Chebyshev pseudospectral method assuming no-slip conditions at the channel walls. For the phase field ϕ, a zero flux of the chemical potential and a fixed contact angle of $\pi/2$ rad are employed. These conditions lead to

$$\mathbf{u}(z=\pm h) = \mathbf{0}, \quad \frac{\partial\phi}{\partial z}(z=\pm h) = 0, \quad \frac{\partial^3\phi}{\partial z^3}(z=\pm h) = 0. \tag{12}$$

Periodicity is applied for both $\mathbf{u}$ and ϕ in streamwise and spanwise directions (x and y). Note that the boundary conditions applied to ϕ directly imply the total conservation of the phase field over time, i.e., $\frac{d}{dt}\int \phi \, dV = 0$.

The computational domain has dimensions $L_x \times L_y \times L_z = 4\pi h \times 2\pi h \times 2h$ and is discretized using $N_x \times N_y \times N_z = 512 \times 256 \times 257$ collocation points. As an initial condition, we injected $N_0 = 256$ drops inside a fully developed turbulent channel flow at $\mathrm{Re}_\tau = 150$. Drops are initially released on two different planes (128 drops for each plane) such that the center of mass of each drop is at 75 wall units from the wall. In wall units, the initial diameter of a drop is $D = 90$, which gives a volume fraction of $\varphi = \frac{V_d}{V_d+V_c} = 0.183$, where V_c and V_d are respectively the volume of the continuous and of the dispersed phase (drops). To resolve the complex drop-turbulence interaction, the drop interface must be carefully described. In the present work, we use a minimum of three points to describe the interface (note that in the wall-normal direction, where the grid is finer, we use five to seven grid points). Considering the constraint of having at least three points to describe the interface, we set $\mathrm{Ch} = 0.0185$ and $\mathrm{Pe} = 162.2$ [31,32].

Simulations are run at a given Reynolds number ($\mathrm{Re}_\tau = 150$) and assuming three different values of We: We = 0.75, 1.5, and 3.0. For each value of We, we consider five different values of the viscosity ratio λ: $\lambda = 0.01$, 0.1, 1, 10, and 100. This gives a total of 15 simulations to cover the entire parameter range. Note that the value of Re_τ employed here is rather low, with the adopted grid making the simulations over-resolved. However, due to the complexity represented by the multiphase flow description, the computational requirements are much larger than for a single phase simulation. An overview of the main simulation parameters is given in Table I.

III. RESULTS AND DISCUSSION

A. Mean velocity of the multiphase mixture

In a multiphase mixture, the transport of large drops with a given surface tension and with an internal viscosity different from that of the carrier flow may influence the macroscopic behavior of the system. In our experiments, for all cases reported in Table I, we observe a modest drag reduction corresponding to an overall flow rate increase in the range 2–4 %. In Fig. 1, the wall-normal

TABLE I. Summary of the simulation parameters ($\mathrm{Re}_\tau = 150$ for all simulations).

	Simulations														
	S1	S2	S3	S4	S5	S6	S7	S8	S9	S10	S11	S12	S13	S14	S15
We	0.75	0.75	0.75	0.75	0.75	1.50	1.50	1.50	1.50	1.50	3.00	3.00	3.00	3.00	3.00
λ	0.01	0.1	1	10	100	0.01	0.1	1	10	100	0.01	0.1	1	10	100

behavior of the mean velocity profile of the multiphase mixture (drops and carrier flow) is shown at four different time instants ($t^+ = 0$, 500, 1000, and 1500). Figures 1(a), 1(b), and 1(c) refer to We = 0.75, We = 1.50, and We = 3.00, respectively. For each value of We, we show only results at $\lambda = 1$ (results at different λ bear only minor quantitative changes that do not add to the discussion). The mean velocity is obtained by averaging the entire flow field (velocities in both phases) along the streamwise and the spanwise directions. All the simulations are initialized with the same velocity field taken from a preliminary simulation of a single phase channel flow at the same Re_τ. As a consequence, at $t^+ = 0$ (solid line), the mean velocity profile for all the simulations collapses onto the classical law of the wall ($u^+ = z^+$ and $u^+ = 2.5 \ln z^+ + 5.5$). As soon as drops are injected inside the channel, they interact with the carrier flow, increasing the mean velocity in the central part of the channel (overshooting of the mean velocity for $z^+ > 30$). Note that, since the driving pressure gradient is kept constant in all our simulations, an increase in the mean velocity indicates a decrease of the friction factor at the wall (drag reduction). By contrast, we observe only negligible flow modifications close to the wall (only for We = 3 a slight increase of $\langle u^+ \rangle$ is observed, which, however, does not represent a significant variation). We remark here that, in accord with previous observations [33] and with this present work, deformable drops tend to stay away from the walls, suggesting that the applied pressure drop is balanced just by the fluid shear stresses at the two walls. In this way, our previous plots on the average velocity of the mixture can have a general significance from the drag reduction viewpoint.

B. Drop dynamics in turbulence

The dynamics of liquid drops immersed in a turbulent flow field is the result of a complex interaction between destabilizing actions due to shear and normal stresses at the drop interface and the stabilizing ones due to surface tension (which tends to preserve drop sphericity). Depending on the relative magnitude of destabilizing and stabilizing actions, drops deform, break, and coalesce. When a viscosity difference between the liquid drops and the external fluid ($\lambda \neq 1$) exists, the picture becomes more complex and the internal viscosity of the drops (η_d) plays an active role in controlling the overall drop dynamics [34,35]. A qualitative representation of such a complex mutual interaction between drops and turbulence is given in Fig. 2. It is apparent that drops (colored in blue) are deformed and advected by the carrier flow (here represented by the flow stream traces colored by the local value of the turbulent kinetic energy of the flow, $E_{k,\mathrm{tot}}$). At the same time, they try to maintain their minimal energy and spherical shape, and they actively modify the flow field. In the following we specifically focus on the role of surface tension (We) and viscosity ratio (λ) on the drop dynamics in a turbulent wall-bounded flow.

1. Influence of viscosity on the number of drops

When a swarm of liquid drops is injected in a turbulent liquid flow, simultaneous coalescence and breakup events are likely to occur [12,20] with their balance ultimately determining the number of drops. To visualize the relative importance of these phenomena we therefore compute the time behavior of the number of drops, $N(t)$, for the different cases considered. Results for $N(t)$ are shown in Fig. 3 and are normalized by the initial number of drops, N_0. Figures 3(a), 3(b), and 3(c) refer

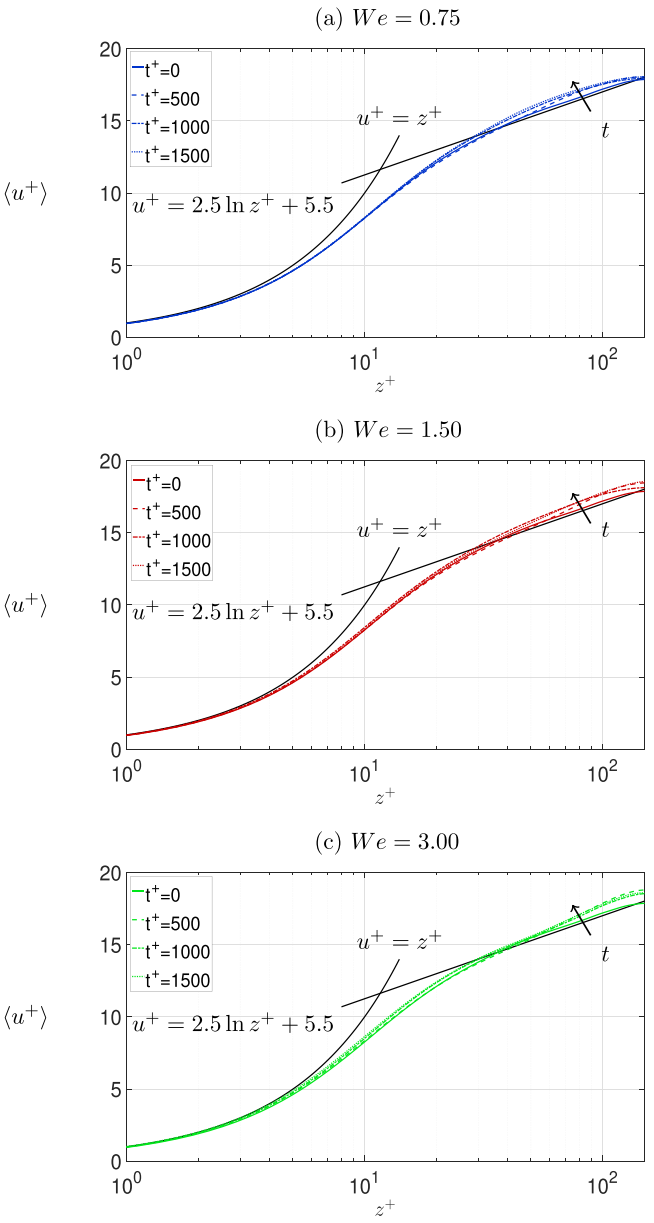

FIG. 1. Wall-normal behavior of the mean streamwise velocity of the mixture (drops and carrier flow) at four different time instants. (a) We = 0.75, (b) We = 1.5, and (c) We = 3. For each value of We results are only shown for $\lambda = 1$. The initial velocity profile (solid line, $t^+ = 0$) is obtained from a preliminary simulation of a single phase flow at the same Re_τ. The behavior of the analytical profile describing the law of the wall is also shown for comparison.

to We = 0.75, We = 1.5, and We = 3, respectively. For each value of We, the drop behavior for all the viscosity ratios ($\lambda = 0.01$, 0.1, 1, 10, and 100) is considered.

For We = 0.75, and regardless of the value of λ, $N(t)/N_0$ decreases monotonically in time. In particular, there is an initial stage (up to $t^+ \simeq 1000$) in which $N(t)/N_0$ decreases sharply in time, indicating a strong predominance of coalescence over breakup events with the consequent formation

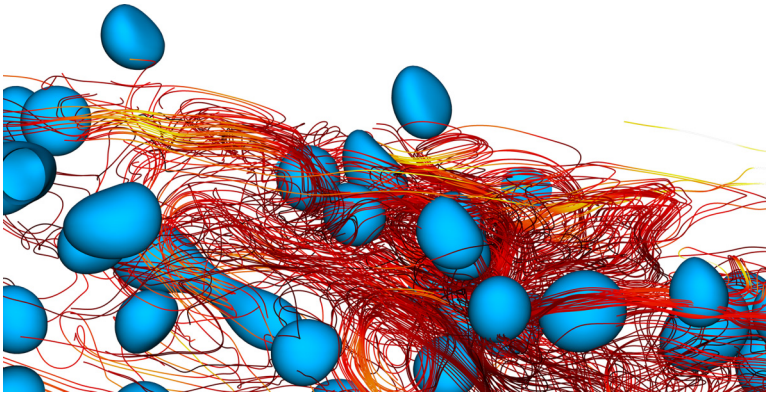

FIG. 2. Instantaneous realization of drop-drop and drop-turbulence interaction. Turbulent flow outside the droplets is highlighted by the stream traces colored by turbulent kinetic energy ($E_{k,\mathrm{tot}}$) level (yellow, low; red, high).

of a few large drops. After this initial stage, the number of drops $N(t)/N_0$ achieves an almost constant value, which indeed barely depends on the value of λ; possibly we observe that the final number of drops, represented by the final plateau, is slightly larger for smaller λ. At this We, the large value of the surface tension compared to inertia hinders drop fragmentation (small deformability), even for small values of their internal viscosity. In Fig. 3(b) we observe the behavior for $\mathrm{We} = 1.5$: as expected, coalescence events dominate during the initial transient, and a statistically steady state is finally achieved in which the number of drops fluctuates around an average value. The effect of viscosity becomes larger in this case: for drops of small viscosity we observe a final number of drops which is about an order of magnitude bigger compared to the case in which the carrier fluid is less viscous than the drops. In Fig. 3(c) we can appreciate the role of drop viscosity at the highest We ($\mathrm{We} = 3$). Drop coalescence dominates [i.e., the number of drops $N(t)/N_0$ decreases in time], until a critical drop size is attained, after which the number of drops achieves a plateau that does depend on λ. It is clear that when the drop viscosity is smaller than that of the carrier fluid ($\lambda < 1$), breakage is favored. By contrast, when the drop viscosity is larger ($\lambda > 1$), coalescence is favored. Of course, viscosity is not surface tension, and even if the effect of increasing drop viscosity (increasing λ) acts as an increase of the surface tension (decrease of We), we must look for the physical mechanism which is ultimately related to turbulence modulation by viscosity [36]. Lower values of the drop viscosity induce larger deformations that eventually cause drop fragmentation (i.e., small drop viscosity is a destabilizing factor). By contrast, large values of drop viscosity represent an extra stability factor for drop dynamics, which indeed induces smaller drop deformation and favors the occurrence of coalescence events. Only for $\lambda = 100$ the dynamics appears somehow different, with the initial transient decay extending up to $t^+ \simeq 800$ and an asymptotic condition characterized by a definitely smaller number of drops. However, this represents an extreme case for which the stabilizing effect due to the large drop viscosity completely balances the small value of the surface tension, resulting in drops having an overall small deformability.

A qualitative representation of the physical mechanism described above is given in Figs. 4 and 5 for the two limiting values of We: Fig. 4 refers to the case $\mathrm{We} = 0.75$, whereas Fig. 5 refers to the case $\mathrm{We} = 3$. For both $\mathrm{We} = 0.75$ and $\mathrm{We} = 3$, we show the drop dispersion and deformation in time (at three different time instants $t^+ = 300$, 600, and 900) for the two extreme cases $\lambda = 0.01$ [Figs. 4(a)–4(c) and 5(a)–5(c)] and $\lambda = 100$ [Figs. 4(d)–4(f) and 5(d)–5(f)]. Together with the drop deformation, we also show the contour map of the $E_{k,\mathrm{tot}}$, a quantity that may be related to drop deformation and dynamics. Note that $E_{k,\mathrm{tot}} = {u'_x}^2 + {u'_y}^2 + {u'_z}^2$ is shown on the channel center plane. In these figures, we observe that the number of drops reduces in time [time increases from Figs. 4(a) to 4(c) and from Figs. 5(a) to 5(c)], regardless of the value of We and λ.

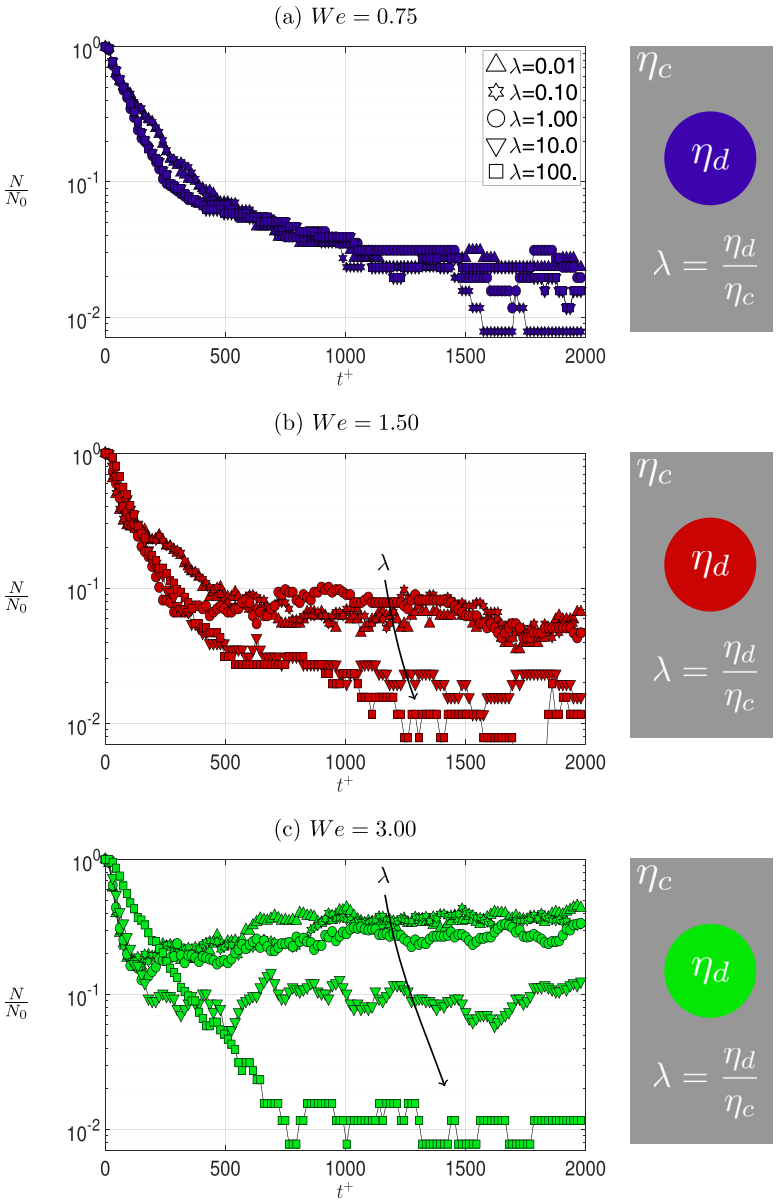

FIG. 3. Time evolution of the normalized number of drops $N(t)/N_0$ for the three different values of We considered in the present study: (a) We = 0.75, (b) We = 1.5, and (c) We = 3. In each panel, results for five different values of λ (λ = 0.01, 0.1, 1, 10, and 100) are shown. A sketch with the definition of λ and the color code is given beside each plot (right part of the figure).

For We = 0.75, the drop shape is rather smooth and slightly dependent on λ. However, for We = 3 (Fig. 5) the situation is remarkably different. The most striking feature observed in this case is the increased drop deformation and the formation of small drop fragments (particularly for λ = 0.01), as a result of recurring and intensive breakup phenomena [34,37]. From the underlying contour maps of $E_{k,\mathrm{tot}}$ (shown in gray scale), we clearly identify the strong coupling between drop deformation and turbulence. Drops, which are first deformed by turbulence fluctuations, induce a turbulence modulation that is somehow linked to drop viscosity, size, and deformation (which in turn

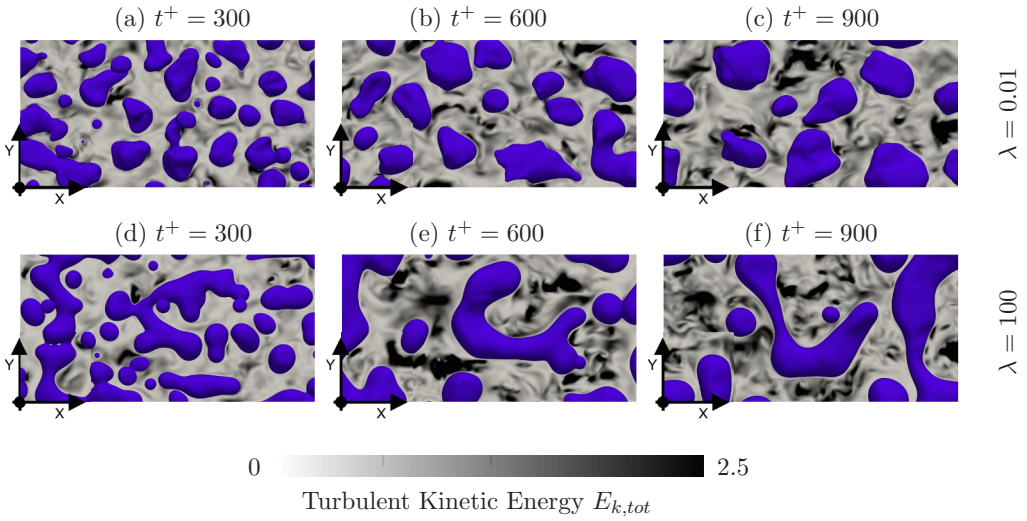

FIG. 4. Drop evolution for We = 0.75 and for the two limiting cases (a)–(c) $\lambda = 0.01$ and (d)–(f) $\lambda = 100$. Each panel refers to a given time instant ($t^+ = 300$, 600, and 900). Contour maps of the $E_{k,\mathrm{tot}}$ computed on a plane passing through the channel center are also shown.

depends on We and λ). In general, the larger is λ, the larger is the drop's effect on the background turbulence.

2. Influence of viscosity on the mean curvature

The mechanism by which a reduction of drop viscosity favors drop breakage can be elucidated further by examining the local interface curvature, since it closely characterizes drop deformation under the action of turbulence, surface tension, and drop-to-fluid viscosity ratio. To compute the

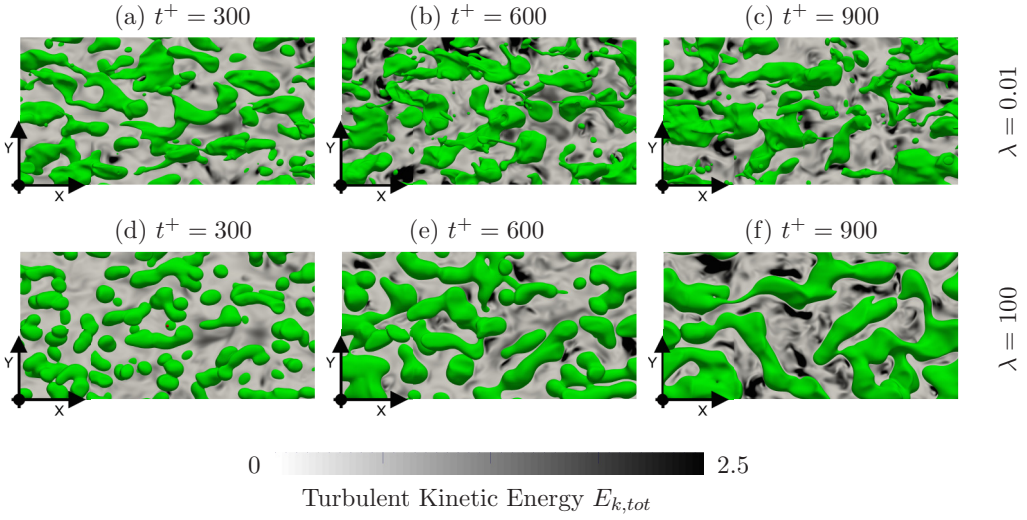

FIG. 5. Drop evolution for We = 3 and for the two limiting cases (a)–(c) $\lambda = 0.01$ and (d)–(f) $\lambda = 100$. Each panel refers to a given time instant ($t^+ = 300$, 600, and 900). Contour maps of the $E_{k,\mathrm{tot}}$ computed on a plane passing through the channel center are also shown.

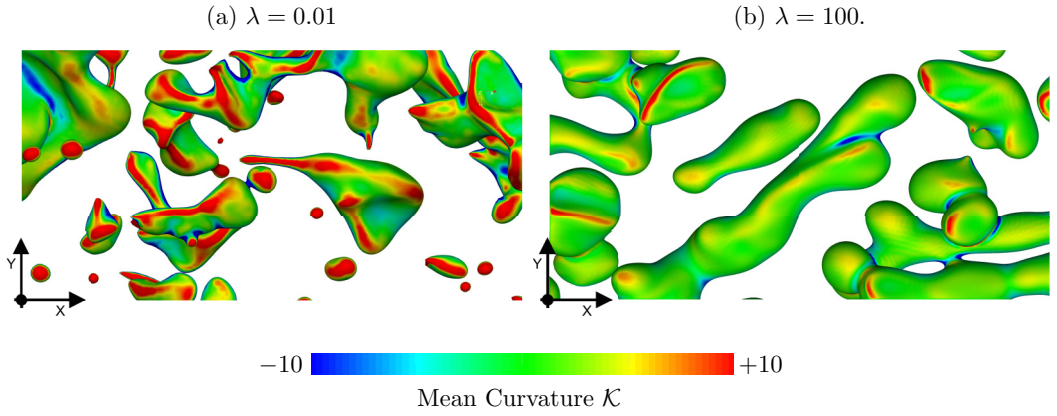

FIG. 6. Mean curvature $\mathcal{K}$ of the drop surface for We = 3 and for the two limiting values of λ: (a) $\lambda = 0.01$ and (b) $\lambda = 100$.

surface curvature, we first identify the drop surface as the isosurface characterized by $\phi = 0$. For each point lying on the drop surface $\phi = 0$, we compute the mean curvature $\mathcal{K}$ as the divergence of the local normal vector $\mathbf{n}$ [38,39]:

$$\mathbf{n} = -\frac{\nabla\phi}{|\nabla\phi|}, \quad \mathcal{K} = \nabla \cdot \left(-\frac{\nabla\phi}{|\nabla\phi|}\right). \tag{13}$$

The mean curvature $\mathcal{K}$ can either be positive or negative, depending on the drop topology (deformation): positive values of $\mathcal{K}$ identify a local convex interface (e.g., a spheroid), whereas negative values of $\mathcal{K}$ identify a local concave shape (e.g., a hyperboloid). Small values of $\mathcal{K}$ indicate a flat interface (or, alternatively, the presence of a saddle point), while large values of $\mathcal{K}$ (both positive or negative) characterize a surface with bumps (positive $\mathcal{K}$) or dimples (negative $\mathcal{K}$), likely indicating possible drop fragmentation. A qualitative picture showing the behavior of the local surface curvature is given in Fig. 6 for the simulation at We = 3 and for the two extreme cases $\lambda = 0.01$ and $\lambda = 100$. Red regions are bumps or small satellite drops, whereas blue regions are dimples and scars at the drop interface. Green regions refer instead to relatively flat interfaces (or saddle points). Unlike the case of small drop viscosity [$\lambda = 0.01$, Fig. 6(a)], where drop fragmentation and increased surface roughness are clearly seen, for large drop viscosity [$\lambda = 100$, Fig. 6(b)], drops are characterized by a smooth surface with small curvature values. This indicates that large drop viscosity increases drop stability against breakage through the increase of drop viscous dissipation [40,41].

To give these observations a more quantitative slant, in Fig. 7 we compute the probability density function (PDF) of the mean curvature $\mathcal{K}$ for all simulated cases. Figure 7(a) refers to the case We = 0.75, whereas Figs. 7(b) and 7(c) refer to the cases We = 1.5 and We = 3, respectively. For each value of We, all λ are shown. We first consider the case We = 0.75 [Fig 7(a)]. We clearly observe that the PDF is asymmetric, with the most probable value occurring for $\mathcal{K} \simeq 0.5$ and with positive curvatures being larger and more probable than negative curvatures. This reflects the observation that at small We the drop shape is not significantly deformed and departs only slightly from its equilibrium (spherical) shape. The effect of changing drop viscosity (λ) is negligible in this case, with all the PDF curves collapsing nicely onto each other. Few differences are observed only for $\lambda = 100$, a case for which the increased drop viscosity hinders drop deformation and reduces the occurrence of large curvature events. Overall, we can safely conclude that, for We = 0.75, effects of drop viscosity on the local curvature remain generally small. The situation changes sharply when larger values of We are considered. In particular, we refer to We = 3, since all the effects we wish to discuss are emphasized in this case (results for We = 1.5 are qualitatively similar, albeit less pronounced). Considering the case We = 3 [Fig. 7(c)], we notice that for small values of the drop

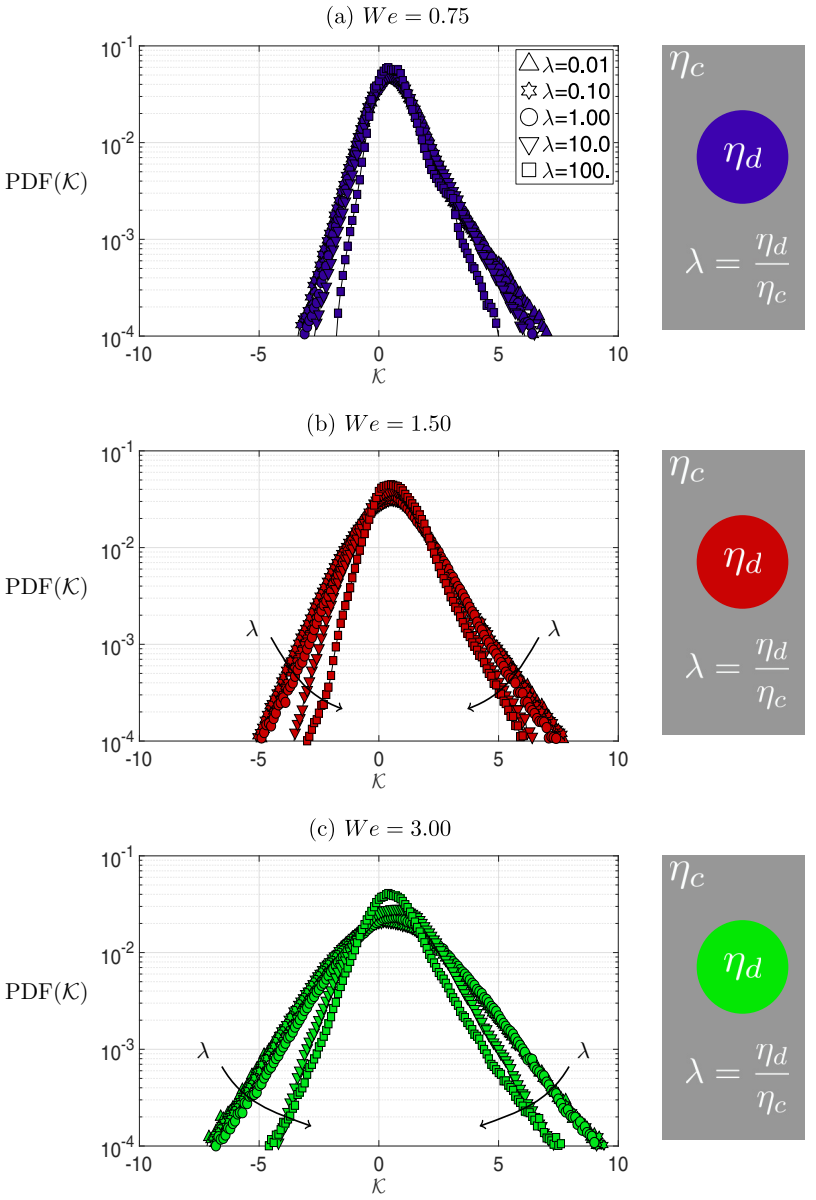

FIG. 7. PDF of the mean curvature $\mathcal{K}$ for the three different values of We considered in the present study: (a) We = 0.75, (b) We = 1.5, and (c) We = 3. In each panel, results for five different values of λ (λ = 0.01, o.1, 1, 10, and 100) are shown. A sketch with the definition of λ and the color code is given beside each plot (right part of the figure).

viscosity ($\lambda < 1$) there is a remarkable increase of the probability of having large curvature events ($|\mathcal{K}| > 5$). This is linked to the physical intuition that for large We and small drop viscosity (small λ) the surface tension is simply too weak to balance the combined effects of external turbulence and small internal viscosity, which ultimately cause a sharp increase of the drop breakup frequency. Interestingly, for large drop viscosity ($\lambda = 10$ and $\lambda = 100$) the shape of the PDF becomes rather similar to that observed for We = 0.75: this indicates that the increased drop viscosity balances the small value of surface tension (We = 3) and prevents drop breakup while promoting drop

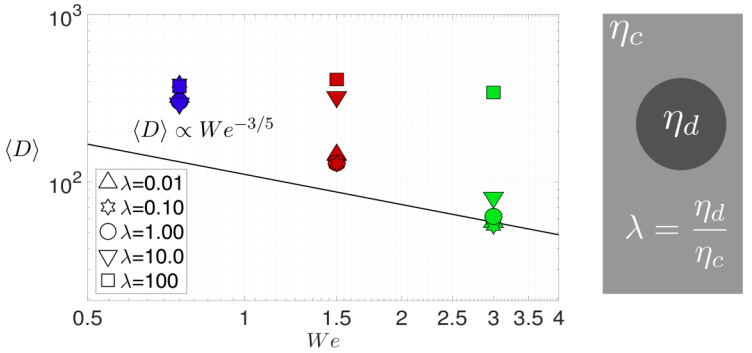

FIG. 8. Mean drop diameter $\langle D \rangle$ obtained for each simulated case (symbols) as a function of We. The theoretical prediction $\langle D \rangle \propto \mathrm{We}^{-3/5}$ given by Hinze [5] is also shown for comparison (solid line). A sketch with the definition of λ is given beside the main panel.

coalescence. These findings have profound effects on the parametrization and modeling of drop breakup and coalesce in turbulence, which is a very important field of research [8,10,11]. It is well established [5] that a critical Weber number $\mathrm{We}_{\mathrm{cr}}$ can be defined such that for $\mathrm{We} > \mathrm{We}_{\mathrm{cr}}$ breakup events dominate, whereas for $\mathrm{We} < \mathrm{We}_{\mathrm{cr}}$ coalesce events dominate. Now, it turned out that for small drop viscosity ($\lambda \leqslant 1$), $\mathrm{We}_{\mathrm{cr}}$ does not significantly depend on λ (negligible viscous dissipation) and $\mathrm{We}_{\mathrm{cr}} \simeq 1.18$ [5]. For small drop viscosity ($\lambda < 1$), we can still retain $\mathrm{We}_{\mathrm{cr}} \simeq 1.18$, since viscous dissipation inside the drop becomes negligible. By contrast, $\mathrm{We}_{\mathrm{cr}}$ is sensitive to an increase of the drop viscosity ($\lambda > 1$). In this case, the large drop viscosity increases drop dissipation and drop stability, a circumstance that ultimately leads to a monotonic increase of $\mathrm{We}_{\mathrm{cr}}$ with λ [5,35,41–43].

3. *Influence of viscosity on critical drop diameter*

As already discussed above, quantifying and controlling drop size distribution in a liquid-liquid mixture is extremely important for the design of efficient emulsification or atomization processes in turbulence [5,8–11,40]. A sound estimate for the diameter of the largest drop (D_{max}) that can be transported without fragmentation in a turbulent environment was given by Hinze [5] for very dilute mixtures (so to neglect possible side effects of coalescence) and assuming that the major contribution to drop breakup is due to velocity fluctuations (dynamic pressure) having wavelength of the order of the drop diameter. For homogeneous isotropic turbulence,

$$D_{\mathrm{max}} = 0.725\left(\frac{\rho}{\sigma}\right)^{-3/5} \varepsilon^{-2/5}. \tag{14}$$

However, for the general case of liquid-liquid mixtures at larger volume fractions, coalescence and breakup events occur simultaneously, a situation which must be taken into consideration to obtain accurate estimates of the collective drop dynamics. In such a complex situation, in which coalescence and breakup may balance each other, a more precise indicator for the drop size is the average drop diameter [19]. From the above considerations, Eq. (14) written for the average drop diameter and expressed in wall units (with the superscript "+" being dropped for ease of notation) becomes

$$\langle D \rangle = 0.725\left(\frac{\mathrm{We}}{\mathrm{Re}_\tau}\right)^{-3/5} \varepsilon^{-2/5}, \tag{15}$$

where the dissipation ϵ, which is in general a function of the wall distance, is here evaluated at the center of the channel (where drops preferentially stay [20,44]). The theoretical behavior of $\langle D \rangle$ described by Eq. (15) is shown in Fig. 8 as a function of We for all the simulated cases. We immediately notice that our results support the validity of Hinze's models, but only for large We and small drop viscosity (when breakups essentially control the dynamics). This is reasonable since the model

is developed assuming negligible coalescence effects (large We) and negligible viscous dissipation (small λ). By contrast, a more complex dependency of the results on We and λ is observed for small We and large λ. Further experimental and numerical campaigns are therefore required to obtain a reliable value of this prefactor for different flow configurations (at present, indicative values of the prefactor can be found for liquid-liquid emulsions in stirred tank reactors [40,41]).

IV. CONCLUSIONS

Drop dynamics in turbulence is a complex phenomenon characterized by the competition between the destabilizing action of turbulence (which deforms and eventually brings the drops to breakage) and the stabilizing action of surface tension (which tends to preserve the drops' integrity). When drop viscosity is different from that of the carrier fluid, the picture becomes even more complex since drop viscous dissipation can become important. In this paper, we precisely focused on the complex interplay between surface tension (We) and drop-to-fluid viscosity ratio (λ), which determines breakage and coalescence of large deformable drops in turbulence. Specifically, we studied the drop dynamics using direct numerical simulations of turbulence coupled with a PFM. We considered three different values of We ($We = 0.75$, 1.5, and 3) and five different values of λ ($\lambda = 0.01$, 0.1, 1, 10, and 100). In all the cases analyzed in the present study, we observed a small increase of the flow rate of the mixture, in the range 2–4 %. We examined also the effect of drops on the average velocity of the mixture (drops and carrier flow) and we observed that, regardless of the value of the physical parameters (λ and We), the average velocity of the mixture increases in time. This is an indication that turbulent kinetic energy is absorbed by drops (i.e., kinetic energy is converted into drop deformation) and induces an overall drag reduction of the flow. Then we focused more closely on drop dynamics. For the base case $\lambda = 1$, we observed that drop dynamics is dominated by coalescence for small We (We < 1), with breakup events entering the picture only for increasing We (We > 1). Interestingly, we found that this situation is selectively modified for $\lambda \neq 1$. For small We (We < 1), drop deformability remains small and the viscosity ratio λ does not influence the coalescence or breakup rate. For larger We (We > 1), drop deformability is increased and the viscosity ratio λ can significantly alter the coalescence and breakup dynamics. In particular, we observed that increasing drop viscosity reduces strongly the breakup rate (and increases the coalescence rate), very much like a reduction of We does. We linked this result to the increased value of the drop viscous dissipation which ultimately increases drop stability. Viscosity gradients across the interface of the drops act as modulators of the local shear stresses and can amplify or damp the inertial turbulence perturbations. Finally, we have been able to compare our results against the theory developed by Hinze [5] to predict the size of a swarm of droplets in turbulence. Our data confirm the predictions [5] at small λ (drop viscosity smaller than fluid viscosity), which is the case analyzed by Hinze. Further analyses are required to examine the phenomena at larger values of drop-to-fluid viscosity ratios.

ACKNOWLEDGMENTS

Support from EU FP7 Nugenia-Plus project (Grant No. 604965), from PRIN (under Grant No. 2006098584 004) and from Regione Autonoma Friuli Venezia Giulia under grant PAR FSC 2007/2013 are gratefully acknowledged. CINECA supercomputing center (Bologna, Italy) and Vienna Scientific Cluster (Vienna, Austria) are also gratefully acknowledged for generous allowance of computer resources.

[1] J. Wu, J. Lu, C. Wilson, Y. Lin, and H. Lu, Effective liquid-liquid extraction method for analysis of pyrethroid and phenylpyrazole pesticides in emulsion-prone surface water samples, J. Chromatogr. A **1217**, 6327 (2010).

[2] D. D. Joseph, M. Renardy, and Y. Renardy, Instability of the flow of two immiscible liquids with different viscosities in a pipe, J. Fluid Mech. **141**, 309 (1984).

[3] K. Chen, R. Bai, and D. D. Joseph, Lubricated pipelining. Part 3: Stability of core-annular flow in vertical pipes, J. Fluid Mech. **214**, 251 (1990).
[4] S. Ahmadi, A. Roccon, F. Zonta, and A. Soldati, Turbulent drag reduction in channel flow with viscosity stratified fluids, Comput. Fluids (2016), doi: 10.1016/j.compfluid.2016.11.007.
[5] J. O. Hinze, Fundamentals of the hydrodynamic mechanism of splitting in dispersion processes, AIChE J. **1**, 289 (1955).
[6] P. H. Clay, The mechanism of emulsion formation in turbulent flow: Part I, Proc. R. Acad. Sci. **43**, 852 (1940).
[7] P. H. Clay, The mechanism of emulsion formation in turbulent flow: Part II, Proc. R. Acad. Sci. **43**, 979 (1940).
[8] H. T. Chen and S. Middleman, Drop size distribution in agitated liquid-liquid systems, AIChE J. **13**, 989 (1967).
[9] C. Y. Wang and R. V. Calabrese, Drop breakup in turbulent stirred-tank contactors. Part II: Relative influence of viscosity and interfacial tension, AIChE J. **32**, 667 (1986).
[10] C. A. Sleicher, Maximum stable drop size in turbulent flow, AIChE J. **8**, 471 (1962).
[11] S. B. Collins and J. G. Knudsen, Drop-size distributions produced by turbulent pipe flow of immiscible liquids, AIChE J. **16**, 1072 (1970).
[12] R. Shinnar, On the behaviour of liquid dispersions in mixing vessels, J. Fluid Mech. **10**, 259 (1961).
[13] J. Qian and C. K. Law, Regimes of coalescence and separation in droplet collision, J. Fluid Mech. **331**, 59 (1997).
[14] N. Ashgriz and J. Y. Poo, Coalescence and separation in binary collisions of liquid drops, J. Fluid Mech. **221**, 183 (1990).
[15] J. D. Paulsen, R. K. Carmigniani, A. Kanman, J. C. Burton, and S. R. Nagel, Coalescence of bubbles and drops in an outer fluid, Nat. Commun. **5**, 3182 (2014).
[16] W. J. Howarth, Coalescence of drops in a turbulent flow field, Chem. Eng. Sci. **19**, 33 (1964).
[17] Greg A. Voth and Alfredo Soldati, Anisotropic particles in turbulence, Annu. Rev. Fluid Mech. **49**, 249 (2017).
[18] D. Qian, J. B. McLaughlin, K. Sankaranarayanan, S. Sundaresan, and K. Kontomaris, Simulation of bubble breakup dynamics in homogeneous turbulence, Chem. Eng. Commun. **193**, 1038 (2006).
[19] P. Perlekar, L. Biferale, M. Sbragaglia, S. Srivastava, and F. Toschi, Droplet size distribution in homogeneous isotropic turbulence, Phys. Fluids **24**, 065101 (2012).
[20] L. Scarbolo, F. Bianco, and A. Soldati, Coalescence and breakup of large droplets in turbulent channel flow, Phys. Fluids **27**, 073302 (2015).
[21] A. E. Komrakova, D. Eskin, and J. J. Derksen, Numerical study of turbulent liquid-liquid dispersions, AIChE J. **61**, 2618 (2015).
[22] R. Skartlien, E. Sollum, and H. Schumann, Droplet size distributions in turbulent emulsions: Breakup criteria and surfactant effects from direct numerical simulations, J. Chem. Phys. **139**, 174901 (2013).
[23] M. S. Dodd and A. Ferrante, On the interaction of Taylor length scale size droplets and isotropic turbulence, J. Fluid Mech. **806**, 356 (2016).
[24] L. Scarbolo, D. Molin, P. Perlekar, M. Sbragaglia, A. Soldati, and F. Toschi, Unified framework for a side-by-side comparison of different multicomponent algorithms: Lattice Boltzmann vs. phase field model, J. Comput. Phys. **234**, 263 (2013).
[25] D. M. Anderson, G. B. McFadden, and A. A. Wheeler, Diffuse interface methods in fluid mechanics, Annu. Rev. Fluid Mech. **30**, 139 (1998).
[26] D. Jacqmin, Calculation of two-phase Navier-Stokes flows using phase-field modeling, J. Comput. Phys **155**, 96 (1999).
[27] P. Yue, J. Feng, C. Liu, and J. Shen, A diffuse-interface method for simulating two-phase flows of complex fluids, J. Fluid Mech. **515**, 293 (2004).
[28] V. E. Badalassi, H. D. Ceniceros, and S. Banerjee, Computation of multiphase systems with phase field models, J. Comput. Phys. **190**, 371 (2003).
[29] J. Kim, Phase-field models for multi-component fluid flows, Commun. Comput. Phys. **12**, 613 (2012).

[30] X. Zheng, H. Babaee, S. Dong, C. Chryssostomidis, and G. E. Karniadakis, A phase-field method for 3D simulation of two-phase heat transfer, Int. J. Heat Mass Transf. **82**, 282 (2015).
[31] F. Magaletti, F. Picano, M. Chinappi, L. Marino, and C. M. Casciola, The sharp-interface limit of the Cahn-Hilliard/Navier-Stokes model for binary fluids, J. Fluid Mech. **714**, 95 (2013).
[32] P. Yue, C. Zhou, and James J. Feng, Sharp-interface limit of the Cahn-Hilliard model for moving contact lines, J. Fluid Mech. **645**, 279 (2010).
[33] J. Lu and G. Tryggvason, Effect of bubble deformability in turbulent bubbly upflow in a vertical channel, Phys. Fluids **20**, 040701 (2008).
[34] Ronnie Andersson and Bengt Andersson, On the breakup of fluid particles in turbulent flows, AIChE J. **52**, 2020 (2006).
[35] R. D. Cohen, Brief communication, Int. J. Multiphase Flow **20**, 211 (1994).
[36] F. Zonta, C. Marchioli, and A. Soldati, Modulation of turbulence in forced convection by temperature-dependent viscosity, J. Fluid Mech. **697**, 150 (2012).
[37] C. D. Eastwood, L. Armi, and J. C. Lasheras, The breakup of immiscible fluids in turbulent flows, J. Fluid Mech. **502**, 309 (2004).
[38] Rutherford Aris, *Vectors, Tensors and the Basic Equations of Fluid Mechanics* (Dover, New York, 1989).
[39] Y. Sun and C. Beckermann, Sharp interface tracking using the phase-field equation, J. Comput. Phys. **220**, 626 (2007).
[40] K. Arai, M. Konno, Y. Matunaga, and S. Saito, Effect of dispersed-phase viscosity on maximum stable drop size for breakup in turbulent-flow, J. Chem. Eng. Jpn. **10**, 325 (1977).
[41] Parichay K. Das, Prediction of maximum stable diameter of viscous drops in a turbulent dispersion, Chem. Eng. Technol. **19**, 39 (1996).
[42] L. P. Hsiang and G. M. Faeth, Near-limit drop deformation and secondary breakup, Int. J. Multiphase Flow **18**, 635 (1992).
[43] H. A. Stone, Dynamics of drop deformation and breakup in viscous fluids, Annu. Rev. Fluid Mech. **26**, 65 (1994).
[44] L. Scarbolo, F. Bianco, and A. Soldati, Turbulence modification by dispersion of large deformable droplets, Eur. J. Mech. B Fluids **55**, 294 (2016).